Electroabsorption measurements of interfaces in a-Si:H/a-SiO$_x$:H and a-Si:H/a-SiN$_x$:H multilayer films

C. B. Roxlo and B. Abeles

Exxon Research and Engineering Company, Corporate Research-Science Laboratories, Clinton Township, Route 22 East, Annandale, New Jersey 08801

We report electroabsorption measurements on amorphous multilayer films made from alternating layers of a-Si:H and a-SiO$_x$:H or from a-Si:H and a-SiN$_x$:H. We observe built-in electric fields (as large as 4×10^5 V/cm) associated with an asymmetric charge distribution in the layers. This asymmetry shows that the electrical properties of the interface depend strongly on the order of deposition. In the a-Si:H/a-SiO$_x$:H system the data are well described by a conduction-band offset which is greater when silicon is deposited onto oxide than when oxide is deposited onto silicon. The difference in offsets is 170 meV when the oxide is made from a mixture of SiH$_4$ and N$_2$O and 220 meV when the oxide is formed entirely through the plasma oxidation of part of the underlaying a-Si:H layer. The a-Si:H/a-SiN$_x$:H multilayers have charges concentrated at defects near the silicon-on-nitride interface. We also determine sublayer thicknesses from the refractive index. These data show that the growth rate increases dramatically when the deposition gas is changed to include N$_2$O, due to oxidation of the a-Si:H layer. Interruption of the plasma during the gas interchange prevents the deposition of substoichiometric oxide and changes the film properties.

I. INTRODUCTION

Semiconductor interfaces are of critical importance in electronic devices. Interface defects can degrade the performance of solar cells, lasers, transistors,[1] and photoreceptors,[2] for example. Amorphous semiconductor multilayer or superlattice systems[3,4] provide an opportunity to study interfaces in amorphous materials due to the large (>100) number of interfaces; in fact, interfaces dominate a number of the macroscopic properties of these systems. Examples in the Si/SiN$_x$ system are high conductivity parallel to the layers due to transfer doping[5] and luminescence efficiency limited by interface recombination centers.[6]

Interface-defect densities have been determined in these materials using a number of spectroscopic techniques, such as midgap optical absorption,[5] electron-spin resonance,[7] luminescence efficiency,[8] and conductivity.[5] These techniques give estimates for the interface defect densities which vary from 10^{10} to 10^{12} cm^{-2}. Hydrogen-concentration measurements and infrared spectroscopy show 10^{15} cm^{-2} extra hydrogen atoms at the interface.[9] We have shown previously[10,11] that electroabsorption spectroscopy can also be used to detect charged interface defects. This is done by a measurement of the built-in fields created by these defects. This technique is distinct from others in two ways: It is sensitive only to charged defects, and it measures the *difference* in charge between two adjacent interfaces. In other words, only those interface charges which depend upon the order of deposition of the sublayers are observed. We observe built-in electric fields of up to 4×10^5 V/cm, corresponding to an interface charge density of at least 3×10^{12} cm^{-2}.

In this paper we present results of electroabsorption measurements of a-Si:H/a-SiN$_x$:H and a-Si:H/a-SiO$_x$:H

multilayers. We give details of the deposition technique and layer-thickness measurements. We also describe the effect of deposition conditions, such as interruption of the plasma during gas exchange and different methods of oxide deposition, on the electroabsorption effect.

In the a-Si:H/a-SiO$_x$:H materials the charge distribution deduced from the electroabsorption measurements is well described by an interface dipole model, or equivalently, a conduction-band mismatch which varies with order of deposition and depends on the manner in which the oxide layer was prepared. In the nitride multilayers the charge distribution is well modeled by an exponentially decreasing charge density at the interface formed when the a-Si:H layer is deposited on a-SiN$_x$:H. We attribute this charge distribution to strain-relieving defects.

II. EXPERIMENTAL

A. Deposition techniques

The superlattice films were made by plasma-assisted chemical-vapor deposition (PCVD) in a 13.6-MHz capacitive reactor shown schematically in Fig. 1.[12,13] The gases A and B were exchanged in the reactor by synchronously opening and closing two pairs of valves. The ballast pump made it possible to exchange the gases without interrupting the flow. Pure SiH$_4$ was used for the a-Si:H layers and mixtures of 5:1 NH$_3$ to SiH$_4$ used for SiN$_x$:H. The a-SiO$_x$:H films were made either by PCVD using a mixture of 50:1 N$_2$O to SiH$_4$ or by plasma oxidation (PO) of the a-Si:H film with N$_2$O. The gases, at a flow rate of 85 SCCM (standard cubic centimeters per minute) and pressures of 30 mTorr were exchanged in the reactor with a time constant of 1 sec. The rf plasma could be turned off during the gas-exchange time. This proved to be im-
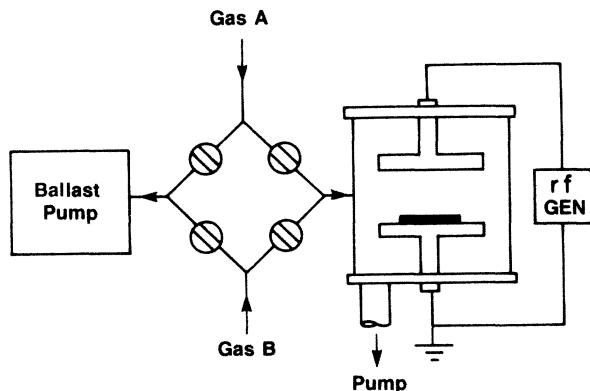
FIG. 1. Plasma CVD system for growth of multilayers

FIG. 2. Silicon sublayer thickness L_s vs deposition time t_s for PCVD Si/SiO$_x$ films.

portant in the case of the silicon—silicon oxide multilayers where a relatively silicon-rich oxide layer grows rapidly during the time when the SiH$_4$ to H$_2$O gas ratio changes. The substrates were held at 240 °C on the anode (grounded electrode) of the reactor. Polished c-Si substrates were used for the infrared measurements, Suprasil quartz for optical measurements, and indium-tin oxide coated glass for electroabsorption samples.

B. Sublayer thickness determination

The thicknesses of the sublayers in the case of the a-Si:H/a-SiN$_x$:H multilayers were determined from the duration of the gas flows and the deposition rates, which were measured separately on thick a-Si:H and a-SiN$_x$:H films. This procedure could not be used in the case of the a-Si:H/a-SiO$_x$:H multilayers because plasma oxidation contributed significantly to the growth of the oxide film in the initial stages of growth. Therefore, we resorted to measurements of the optical index n of the multilayers to determine the thicknesses of the a-Si:H and a-SiO$_x$:H layers using the effective-medium relation

$$n^2 = (n_s^2 L_s + n_o^2 L_0)/(L_s + L_o) ,$$

where n_s, n_o and L_s and L_o are the optical indices and thicknesses of the a-Si:H and a-SiO$_x$:H layers.

Figure 2 shows that the growth of the a-Si:H sublayer is slow for short deposition times t_s. This is because a significant fraction of the a-Si:H film is oxidized in the initial stages of the a-SiO$_x$:H deposition. From the intercept of the straight-line extrapolation of the growth curve in Fig. 2 we estimate about 10 Å of a-Si:H is consumed. The oxidation of the a-Si:H film manifests itself as an initial steep rise in oxide thickness L_o with deposition time t_o as shown in Fig. 3 for the a-SiO$_x$:H layers given by PCVD. (The fast initial growth of the oxide layer on a-Si:H has been observed directly by in $situ$ optical reflectivity measurements.[14]) The thickness of the oxide layer formed by oxidation of the underlaying a-Si:H layer is given by the intercept of the linear extrapolation (dashed line in Fig. 3) of the PCVD growth curve and by the sa-
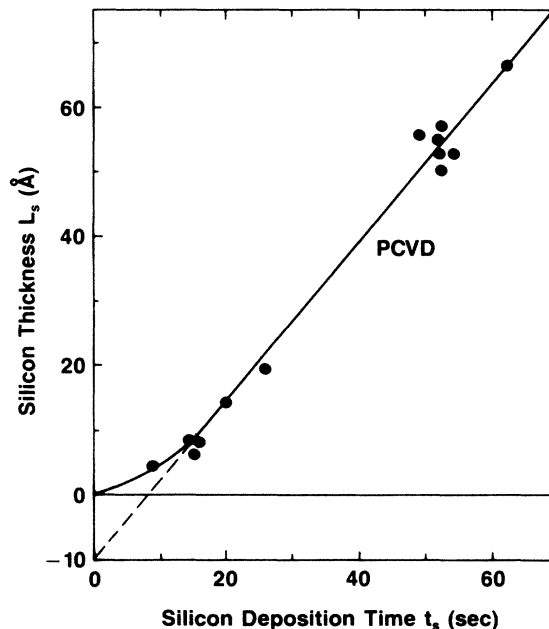
turation value of the PO growth curve in Fig. 3. Both of these values are 17 Å.

To determine the atomic composition of the a-Si:H, a-SiN$_x$:H, a-SiO$_x$:H films and of the multilayers we measured the Si, N, and O concentrations by Rutherford backscattering and used N^{15} nuclear resonant reaction to determine the H concentration. The compositions of the bulk films were SiH$_{0.13}$, SiN$_{1.05}$H$_{0.45}$, and SiO$_{1.85}$H$_{0.09}$. In the case of the multilayers, we measured average compositions because the intrinsic depth resolution of these techniques was insufficient to resolve the variation in x and C_H with a depth scale < 200 Å. The average compositions (Si, N, and O) of the multilayer films agreed with those calculated from the compositions measured on the thick films and the sublayer thicknesses. The multilayers
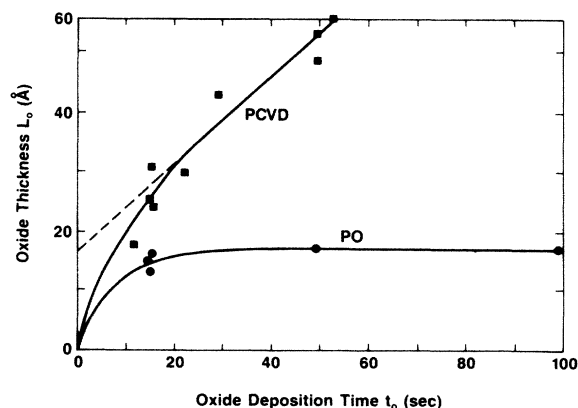

FIG. 3. Oxide sublayer thickness L_o vs oxide deposition time t_o for Si/SiO$_x$ multilayer systems. The two curves are for oxides created in SiH$_4$/N$_2$O plasmas (PCVD) and N$_2$O alone (PO).

had extra hydrogen concentrated at the interfaces. Detailed measurements of the nitride system showed $\sim 10^{15}$ cm^{-2} extra hydrogen atoms at the interface formed when a-Si:H is deposited onto a-SiN$_x$:H.[9]

C. Electroabsorption spectroscopy

The electroabsorption technique consists of monitoring the change in optical transmission near the band-gap energy due to an electric field applied perpendicular to the layers. In crystalline semiconductors[15] the band gap is observed to shift to lower energies with increasing fields. This effect, referred to as the Franz-Keldysh effect,[16] can be attributed to tunneling of carriers into the forbidden gap, where they can absorb photons of energy less then the zero-field gap. In amorphous semiconductors, the situation is theoretically less clear.[17,18] The electroabsorption signal is observed to peak very close to the Tauc optical gap, and it decreases proportionally to the absorption coefficient at lower energies.[19,20] This general behavior has been seen in a wide number of amorphous semiconductors, including a-Si:H (Refs. 21—23) and was observed on all the materials studied here.

In the present experiments we will use electroabsorption to determine built-in electric fields rather than spectroscopic information about the energy bands. This technique has been used by Nanomura and co-workers[24,25] to determine built-in potentials in amorphous silicon solar cells. The technique relies on the fact that the electroabsorption signal is proportional to the square of the electric field. The first harmonic signal then vanishes if an applied dc field cancels out the internal fields, yielding an accurate measure of the built-in potential.

In our apparatus the light from a 1-kW xenon lamp was dispersed in a $\frac{1}{4}$-m monochromator. It was filtered both spatially and with color filters before being focused to a 2-mm spot on the sample. The transmitted light was refiltered before detection with a silicon photodiode. The sample was biased with a 1-kHz sine wave in series with a computer-controlled dc voltage generator. The signal at either the first or second harmonic of the applied voltage was detected using a lock-in amplifier.

The samples were deposited onto substrates coated with indium-tin oxide and a thin (200 Å) layer of a-Si:H doped with 1 at.% P. This provided an ohmic contact to the silicon sublayer which was the sublayer deposited first. The superlattice films were in the thickness range between 0.1 and 3 μm, but usually near 1.0 μm. Semitransparent palladium or platinum dots 2 mm in diameter were used as the top contact. This configuration on an unlayered a-Si:H film had a contact potential of 0.5 V, much less than the built-in potentials measured on the layered films.

It is very important for the analysis of the electrical data that the applied voltages, particularly the ac voltage, be uniformly dropped across the sample. This is expected from the known properties of the superlattice. The 10^{12} Ω cm resistivities observed[12] yield a dielectric relaxation time of $\simeq 1$ sec, while our modulation frequency was 1 kHz or higher. The depletion width[26,27] of bulk a-Si:H is known to be several thousand angstroms, greater than the thickest silicon sublayers used here.

We have confirmed uniform fields in several ways. First, a large number of samples were analyzed when cooled to less than 50 K. At this temperature virtually all charges are frozen in place, unable to react to the applied fields and change the field distribution. Secondly, the ac frequency was varied between 100 Hz and 100 kHz with the sample at room temperature. The measured built-in potentials were changed by less than 10% by these methods, indicating that moving charges did not significantly distort the fields or affect the electroabsorption. Measurements were also made with the dc voltage applied as a 3-msec pulse. Again there was no change, indicating the dc and ac fields are uniform throughout the film.

In this case we can make use of the boundary condition that the applied electric displacement $D = \epsilon E$ is constant. The field is related to the applied voltage by

$$V = \int_0^d \frac{D}{\epsilon} dx \ ,$$

where x is distance normal to the layers, and d is the sample thickness. We will assume that the dielectric constant ϵ in each sublayer is equal to that of an unlayered film: $\epsilon_s = 12\epsilon_0$ in the silicon sublayers and ϵ_i in the insulator sublayers ($\epsilon_i = 7.5\epsilon_0$ for SiN$_x$ and $\epsilon_i = 4\epsilon_0$ in SiO$_x$).[28] The film is made up of N layer pairs, with silicon and insulator sublayers of thicknesses L_s and L_i, respectively. We have

$$D_{\text{app}} = \frac{V_{\text{app}}}{N} \left[\frac{L_s}{\epsilon_s} + \frac{L_i}{\epsilon_i} \right]^{-1} \ , \tag{1}$$

independent of x. This has both dc and ac components

$$D_{\text{app}} = D_{\text{dc}} + D_{\text{ac}} \cos(\omega t) \ , \tag{2}$$

where ω is the modulation frequency.

The total local field is made up of both applied and built-in fields

$$D(x) = D_{\text{app}} + D_{\text{BI}}(x) \ , \tag{3}$$

where the built-in field D_{BI} depends on x due to local charges. The materials considered here are amorphous and therefore locally isotropic. In this case, symmetry requires that the local change in absorption coefficient depends (in lowest order) only on the square of the field

$$\Delta\alpha(x) = \alpha_0(x) K(x) D^2(x) \ , \tag{4}$$

where α_0 is the zero-field absorption coefficient, and K is the electro-optic coefficient. Any terms of $\Delta\alpha$ which are linear in D are not allowed due to the reflection symmetry of an amorphous material. Of course, as we will show, this is not true for the superlattice as a whole due to the asymmetry between the interfaces. This asymmetry is reflected in the spatial dependence of the built-in field $D_{\text{BI}}(x)$.

From the above equations, we find that

$$\Delta\alpha(x) = \alpha_0(x) K(x) [D_{\text{dc}} + D_{\text{ac}} \cos(\omega t) + D_{\text{BI}}(x)]^2 \ . \tag{5}$$

This expression can be separated into terms in the zeroth, first, and second harmonics of $\cos(\omega t)$. In a previous paper,[29] we showed that the measured ratio between the first

and second harmonic terms agrees with that predicted by (5) within 5%. For the purposes of this paper we will require only the first harmonic expansion; it is

$$\Delta\alpha_\omega(x) = 2\alpha_o(x)K(x)[D_{BI}(x) + D_{dc}]D_{ac} , \tag{6}$$

where we have suppressed the $\cos(\omega t)$ time dependence.

The net change in transmission is equal to an average over the sample thickness:

$$\Delta\alpha_\omega = \frac{1}{d}\int_0^d \Delta\alpha_\omega(x)dx . \tag{7}$$

In order to evaluate the contributions of the different sublayers to $\Delta\alpha_\omega$, we must know their optic and electro-optic properties, $\alpha(x)$ and $K(x)$. Electroabsorption measurements taken as a function of energy in Si/SiN$_x$ multilayers have shown that the optical band gap changes abruptly at the interface, changing by more than 0.6 eV in the first 3 Å.[10] A wide number of techniques have shown that the interfaces are abrupt within 5 Å, including Raman scattering,[30] electron microscopy,[31,32] and x-ray diffraction.[3,33] Based on this data we assume that α and K are constant inside each sublayer and shift abruptly at the interface. We therefore take $\alpha(x)=\alpha_s$ and $K(x)=K_s$ in the silicon sublayer and similarly α_i and K_i in the barrier region.

The experiments in this paper were done at photon energies of roughly 2 eV, near the band gap of a-Si:H. Both a-SiN$_x$:H and a-SiO$_x$:H have band gaps greater than 3.5 eV, and their absorption coefficients at 2 eV are less than 100 cm^{-1}. Therefore, any absorption in the barrier regions is negligible ($\alpha_i \approx 0$) and only the silicon sublayers need be considered. Assuming that the built-in fields in each silicon sublayer are identical, (7) reduces to an integral over a single sublayer,

$$\Delta\alpha_\omega = \frac{2\alpha_s K_s N}{d}\int_0^{L_s}[D_{BI}(x) + D_{dc}]D_{ac}dx$$

$$= \frac{2\alpha_s K_s N}{d}D_{ac}\left[D_{dc}L_s + \int_0^{L_s}D_{BI}(x)dx\right] . \tag{8}$$

This can be easily expressed in terms of the built-in potential across a single silicon sublayer,

$$\phi_s = \frac{-1}{\epsilon_s}\int_o^{L_s}D_{BI}(x)dx . \tag{9}$$

Here a positive ϕ_s refers to an electric field which points away from the substrate. The electroabsorption signal (8) can be expressed in terms of the applied and built-in voltages using (1):

$$\Delta\alpha_\omega \sim V_{ac}\left[\phi_s - \frac{V_{dc}}{N}\left[\frac{L_i\epsilon_s}{1+L_s\epsilon_i}\right]^{-1}\right] \tag{10}$$

or

$$\Delta\alpha_\omega \sim V_{ac}[V_{BI} - V_{dc}] , \tag{11}$$

where

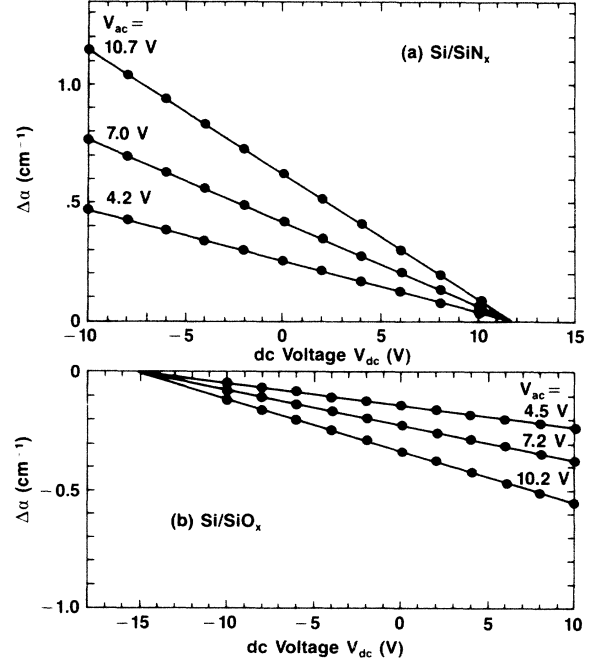$$V_{BI} = N\left[1 + \frac{L_i\epsilon_s}{L_s\epsilon_i}\right]\phi_s \tag{12}$$

FIG. 4. Electroabsorption measurements for (a) a Si/SiN$_x$ multilayer with $L_s=39$ Å, $L_N=46$ Å and $N=125$; (b) a PCVD Si/SiO$_x$ multilayer with $L_s=L_o=50$ Å and $N=110$. $\Delta\alpha$ is plotted vs V_{dc} for three values of V_{ac}. The straight lines are individually fit to each set of points and intersect the x axis at $V_{dc}=V_{BI}$.

is the external voltage which must be applied in order to cancel out the built-in fields in the silicon sublayers.

This simple algebraic expression is obeyed quite accurately in practice. Figure 4 shows the $\Delta\alpha_\omega$ observed in two samples as a function of V_{dc} and V_{ac}. The linear relationship (11) is obeyed within experimental error (1%). The intercept with the horizontal axis of the straight-line fits gives an accurate measure of V_{BI}, from which we can easily calculate the single-layer potential ϕ_s using Eq. (12). Note in Fig. 4 that the built-in potential in the nitride multilayers ($\phi_s > 0$) is opposite to that in the oxides ($\phi_s < 0$).

III. MODEL CHARGE DISTRIBUTIONS

Although ϕ_s is an important parameter for characterizing multilayer device structures, the interface charge and its spatial distribution are more interesting from a physical point of view. In order to derive the charge distribution, it is necessary to measure a number of superlattices and compare the dependence of ϕ_s upon the sublayer thicknesses. This technique relies on the assumption that the interface charge distribution does not change when the sublayer thickness is varied, or at least that it changes in a way that can be included in the model. This assumption cannot be expected to hold when the interfaces are so close together that the interface charges overlap. We conservatively estimate this limit to fall around sublayer thicknesses of 10–20 Å. Above that, the analysis should be valid in the absence of gross changes such as Fermi-level shifts.

In this section we derive the ϕ_s dependence expected from two charge distributions, a simple interface charge, and an interface dipole. Later we will show that the a-Si/a-SiO$_x$ system fits the interface-dipole model quite well. The nitride system is relatively complex but appears to be best fit by a more complicated model which will be described later.

First there are general considerations which any distribution must meet. All the sublayers are identical, so that the net-charge distribution $\rho(x)$ is periodic in x with periodicity $L_s + L_i$. Charge neutrality must be obeyed, so that

$$\int_0^{L_s+L_i} \rho(x)dx = 0 . \tag{13}$$

The built-in fields are then determined from

$$D_{\rm BI}(x) = e \int \rho(x)dx . \tag{14}$$

One additional boundary condition is needed to determine $D_{\rm BI}(x)$, and this condition is imposed by the external contacts. In the absence of an applied voltage, the potential drop across the entire sample (or equivalently across a layer pair) is zero,

$$\int_0^{L_s+L_i} \frac{D_{\rm BI}(x)}{\epsilon(x)} dx = 0 . \tag{15}$$

A. Interface charge model

The simplest possible charge model is one in which a positive charge at one interface is neutralized by an opposite charge at the other interface. This distribution is shown in Fig. 5(a). The actual distribution is

$$\rho(x) = e\sigma[\delta(x) - \delta(x - L_s)] , \tag{16}$$

where σ is the interface charge density and $\delta(x)$ is the Dirac δ function. The field D is a constant in each region and changes at the interfaces by the amount of the surface charge σ. The field in the silicon sublayers is

$$D(0 < x < L_s) = \sigma e \epsilon_s L_i / (\epsilon_s L_i + \epsilon_i L_s) \tag{17}$$

and the built-in potential is

$$\phi_s = \frac{\sigma e L_s L_i}{\epsilon_s L_i + \epsilon_i L_s} . \tag{18}$$

For a given barrier thickness L_i, this potential increases monotonically with increasing L_s until $\phi_s = \sigma e L_i / \epsilon_i$ at large L_s.

In addition to being the simplest possible charge distribution, this model yields the highest ϕ_s for a given interface charge density. In other words, the charge density σ calculated from (18) represents an absolute lower limit on the total charge present for an observed ϕ_s. In the sample shown in Fig. 4(a), the surface charge is $\sigma = 6 \times 10^{11}$ cm^{-2} on the surface where silicon is deposited onto silicon nitride, and an equal and opposite charge on the opposite interface. On other samples, this calculation yields surface charges as high as 3×10^{12} cm^{-2}. The actual total charge is probably even greater than this, because presumably not all the charge is asymmetrically distributed as is indicated by this model. A more detailed description of the charge distribution in Si/SiN$_x$ multilayers is given in Sec. IV B.
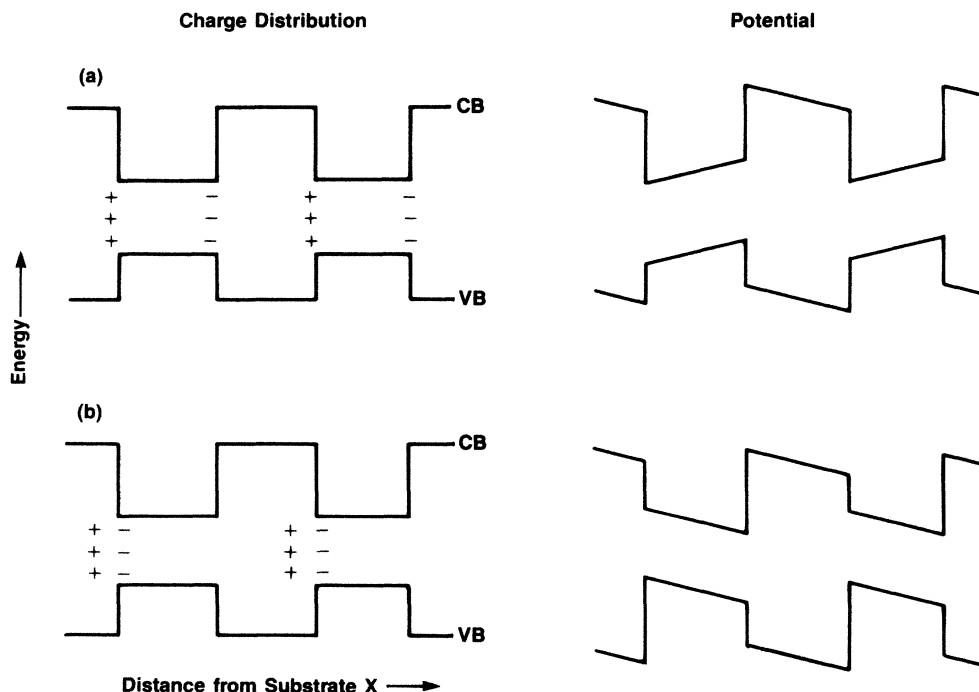
Charge Distribution **Potential**

(a)

(b)

Distance from Substrate X ⟶

FIG. 5. Generalized-model charge distributions for (a) interface charge model; (b) interface dipole model.
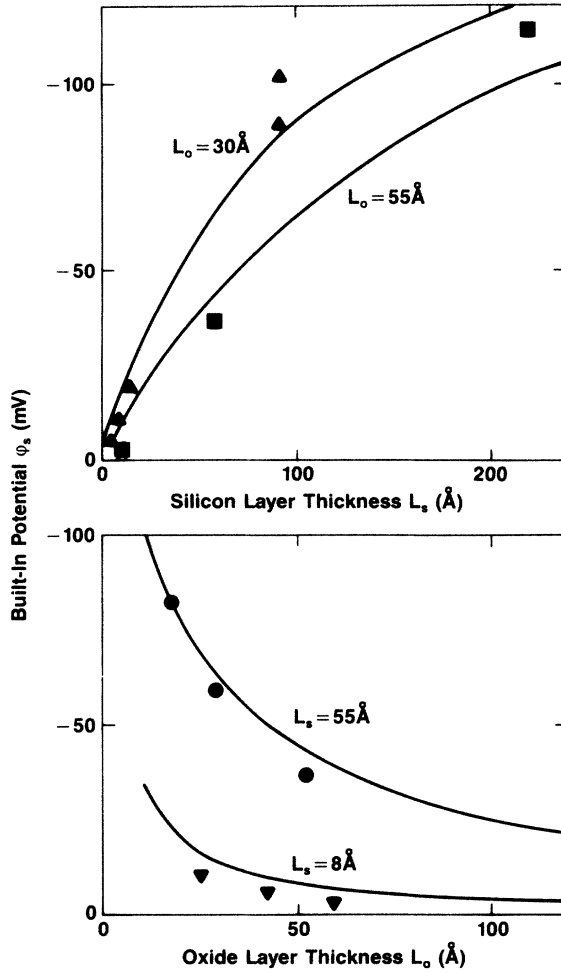
FIG. 6. Built-in potential ϕ_s vs layer thicknesses for PCVD Si/SiO$_x$ multilayers. The lines are a single parameter fit for all four sets of data to the interface dipole model (Eq. 19) shown in Fig. 5(b).

FIG. 7. Built-in potential ϕ_s vs silicon thickness L_s for a series of films with $L_N=27$ Å.

B. Interface-dipole model

Another simple model is that of an interface electric dipole. Although such a charge would presumably exist at both interfaces, only the difference in dipole strength is observed in this experiment. For this reason, we assume that the dipole is located at only one of the interfaces [Fig. 5(b)]. We have located the dipole charge in the insulator region. This is equivalent to having the dipole exactly at the interface, because in both places it is located where electroabsorption at photon energies near the silicon band gap does not experience the field interior to the dipole.

Consider an interface dipole of strength δ (C/cm). This charge produces a step in the potential of intensity $\psi=\delta/\epsilon_i$. This potential step is canceled out through the layer pair by a constant field $D_0=\psi(\epsilon_s\epsilon_i)/L_s\epsilon_i+L_i\epsilon_s$, so that the potential drop across the silicon sublayer is

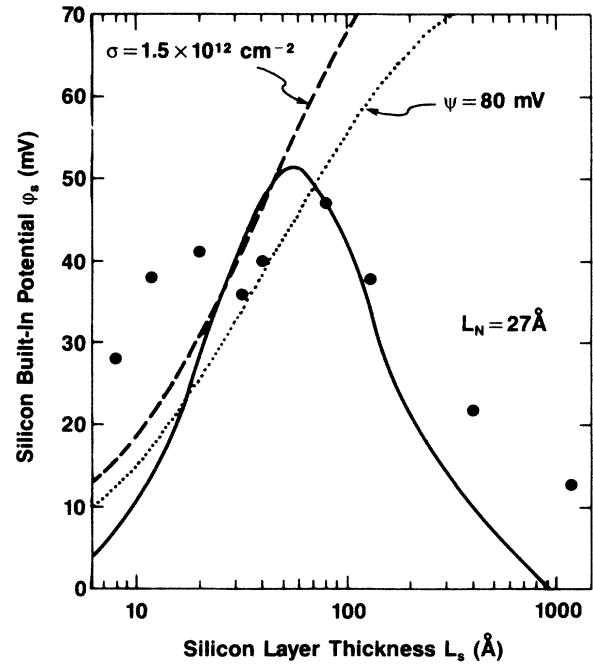$$\phi_s=\psi\frac{L_s\epsilon_i}{L_i\epsilon_s+L_s\epsilon_i}.\qquad(19)$$

The dipole potential ψ is distributed between the two sublayers as between capacitors in series, with each sublayer having a "capacitance" of ϵ/L. For thick silicon sublayers the entire dipole potential is dropped across the silicon sublayer and $\phi_s=\psi$.

Because the effect of the interface dipole is a step in potential, this charge distribution is eqivalent to a change in the conduction-band-edge discontinuity. In other words, the conduction-band-edge mismatch at the interface depends upon the order of deposition.

IV. RESULTS

A. Si/SiO$_x$

Figure 6 shows the built-in potentials obtained from a large number of a-Si:H/a-SiO$_x$:H multilayers with silicon thicknesses varying from 8 to 220 Å and oxides from 15 to 60 Å. To avoid the deposition of a substoichiometric oxide the plasma was interrupted for 10 sec during the gas interchange for all of these samples. It can be seen that ϕ_s increases with increasing silicon thickness and decreases for thicker oxides, as would be expected from an interface dipole. The four curves in Fig. 6 are the values predicted from Eq. (19). All four curves are fitted with only one free parameter, that being the interface-dipole potential of $\psi=170$ mV. The sublayer thicknesses were those determined from the index of refraction. The fit obtained is excellent, the only exception being the somewhat lower than theoretical values obtained on the 8-Å-thick silicon samples. This could easily be due to the finite thickness of the interfaces,[34] which would
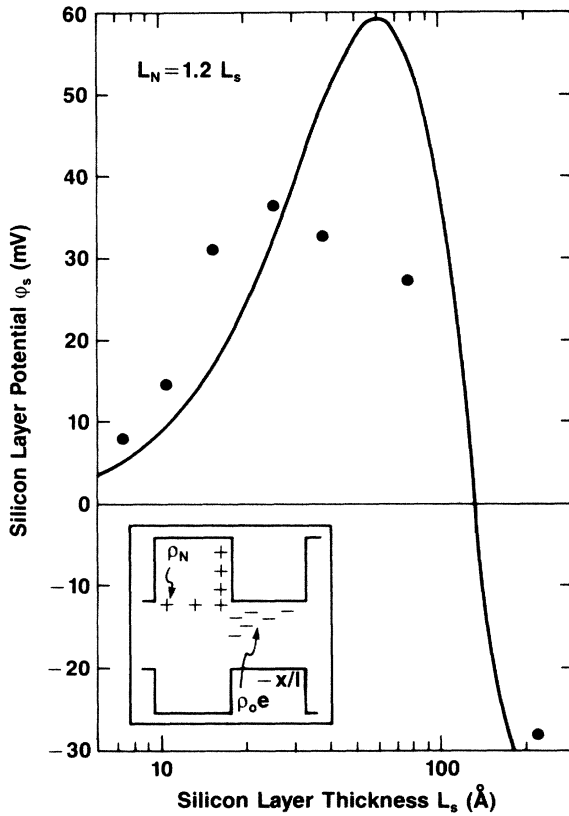
FIG. 8. Built-in potential ϕ_s vs silicon thickness L_s with $L_s = 0.85L_N$.

tend to make the effective silicon thickness for electroabsorption thinner than that measured by the index of refraction.

This result indicates that the oxide-on-silicon interface has a 170-mV-greater conduction band discontinuity than the silicon-on-oxide interface. The data indicate that this interface dipole is located within 5 Å of the interface. To express this potential in terms of charges, assume two surface charges σ separated by $t = 5$ Å. In this case, $\sigma = \psi \epsilon_i / et = 7 \times 10^{12}$ cm^{-2}, a large but not unreasonable value.

B. Si/SiN$_x$

In the case of the a-Si:H/a-SiN$_x$:H superlattices the situation is not so simple. The results we have obtained[10] with a nitride thickness of 27 Å and silicon thicknesses between 8 and 1200 Å are shown in Fig. 7. The two dotted lines are the dependences expected from the interface charge model and the interface dipole model with the "best fit" parameters shown. It can be seen that neither of these two idealized charge distributions fits the data even qualitatively, because they do not predict the decrease in ϕ_s to near zero at large layer thicknesses.

This decrease can be explained by electrons distributed through the silicon sublayer near the interface where the

compensating positive charge is. This would be expected in the case where the charges reside in interfacial defects. Effectively this is very similar to a dipole where the entire dipole charge lies in the silicon; for large L_s the potential across the nitride layers is near zero while the silicon potential has two opposing contributions. To quantify this distribution, let the electron density in the silicon sublayer be

$$n_e = \rho_0 \exp(-x/l) ,$$

where x is distance from the silicon-on-nitride interface. This charge is balanced by a positive interface charge at that interface. This distribution is much like an interface dipole for high L_s, with the positive and negative charges separated by l. But for small L_s the charge is quite similar to a positive interface charge balanced by a constant electron density in the silicon. In this model, the total charge density increases as L_s increases up to $L_s \approx l$. This is reasonable in the Si/SiN$_x$ system where transfer doping is known to be important.

In a previous paper[10] we showed that this distribution gave a reasonable qualitative fit to the series of samples shown in Fig. 7, where $L_N = 27$ Å. In Fig. 8 we show another series where the ratio between layer thicknesses is kept constant, $L_s = 0.85L_N$. These samples give more detailed information about the charge distribution in the nitride. This data is well explained by the model above for $L_N \lesssim 40$ Å, but for greater nitride thicknesses the observed potential is much less. This is due to the fact that the positive charge is distributed throughout the nitride sublayer; it can be explained by a distribution which has $\rho_N = 7 \times 10^{17}$ cm^{-3} charges distributed uniformly through the layer. The remaining positive charge required to balance the electrons in the silicon layer is located at the interface. This charge distribution is shown as the inset in Fig. 8. Electrostatic calculations similar to those in Sec. III above give the potential expected from this model as

$$\phi_s = \frac{\rho_s l L_s L_N e^{-Ls/l} + \rho_s l^2 L_N (e^{-Ls/l} - 1) - 2\rho_N L_N^2 L_s}{L_s \epsilon_N + L_N \epsilon_s} .$$

This fit is shown as the solid curves in Figs. 7 and 8. The parameters used are $\rho_0 = 3 \times 10^{19}$ cm^{-3} and $l = 20$ Å, as in Ref. 10, and $\rho_N = 7 \times 10^{17}$ cm^{-3}. While this model cannot be claimed to be unique, the qualitative fit to the data is good. Both sample sets peak at sublayer thicknesses near 100 Å decreasing to both sides. We also observe that the $L_s = 220$ Å, $L_N = 260$ Å sample has negative ϕ_s, in agreement with the model.

V. EFFECT OF DEPOSITION CONDITIONS

Interrupting the plasma during the interchange of gases prevents the contamination of the film by off-stoichiometry material deposited during the gas interchange. This is very important in the case of the a-Si:H/a-SiO$_x$:H multilayers. This is due to the strong dependence of deposition rate on gas ratio; this rate is low for a gas of pure silane (1.0 Å/sec) or for our gas ratio of 50:1 N$_2$O to SiH$_4$ (0.8 Å/sec). However, at intermediate ratios the deposition rate is much higher, as much as 4 Å/sec at 1:1 N$_2$O to SiH$_4$. This means that a film depo-

sited with a continuous plasma will have several angstroms of silicon-rich oxide deposited at each interface, even with our gas interchange time of 1 sec. Such an interface is expected to be graded from one side to the other, and may be undesirable in the preparation of multilayer films with high-quality abrupt interfaces. Indeed, we observed that oxide films prepared with a continuous plasma had very small optical bandgap shifts. A film with 12-Å-thick silicon layers had a bandgap less than 0.05 eV greater than bulk a-Si:H, as opposed to the 0.3-eV shift observed in the interrupted plasma.

No detectable deposition occurs within the 10 sec the plasma is interrupted during the gas interchange. This can be seen using *in situ* reflectivity.[34] We have confirmed this by depositing a film which was exposed to N_2O between the deposition of layers of a-Si:H, without plasma ignition during the oxide exposure. This film had no appreciable oxide content, and was virtually indistinguishable from a bulk a-Si:H film. This shows that no appreciable deposition occurs when the plasma is off, and there is no contamination of the a-Si:H layer by desorbed N_2O. As discussed above in Sec. II B, an approximately 17-Å-thick silicon oxide layer is formed within 15 seconds after the plasma is turned on when the SiO_2 deposition begins. If an N_2O/SiH_4 mixture is used, a-SiO_x:H deposition continues onto this material. If only N_2O is used in the gas, the deposition stops at this point.

The plasma-oxidized films are observed to have a higher band edge discontinuity than the equivalent films grown by CVD (220 versus 170 mV). This reflects an even stronger asymmetry between the interfaces in the plasma oxidized films. Essentially these materials have one interface which is created through the oxidation of already existing a-Si:H, whereas the opposite interface is a-Si:H grown onto an oxide substrate. It is perhaps not surprising that in this case the two interfaces have different properties.

In the case of the silicon—silicon nitride multilayers, no difference (< 10%) was observed in the built-in potential between films which had the plasma interrupted or continuous between layers. Also photothermal deflection spectroscopy measurements of the density and absorption spectra of subband-gap defects showed that the films were identical within experimental error. In the case where the plasma was interrupted, a 10-sec period was allowed for the gases to change. Because the gas-holding time in this reactor was less than 1 sec, this is ample time for the removal of all ammonia from the gas phase. The similarity between this sample and one with continuous plasma deposition shows that nitrogen contamination of the silicon layers is unimportant.

VI. DISCUSSION

In this laboratory we have prepared amorphous multilayers out of a-Si:H alternating with four different materials: a-SiN_x:H, a-SiO_x:H, a-SiC_x:H, and a-Ge:H. It is of interest to rank these systems in order of interface defect density. In the germanium and carbide multilayers, only a few samples have been tested so that it is not possible to model the thickness dependence. For this reason we compare different systems on the basis of interface charge

density, as described in Sec. III A above. As we showed above, this is not the best description of the a-Si:H/a-SiO_x:H system, but can be used roughly for comparison purposes as long as we compare samples of similar (~20 Å) thicknesses. In the nitrides this charge was as high as $\sigma = 3 \times 10^{12}$ cm^{-2}. In the oxides the fields were of opposite sign with $\sigma \sim -3 \times 10^{11}$ cm^{-2} for deposited oxides and $\sigma \sim -10^{12}$ cm^{-2} for plasma-oxidized material.

The three carbide multilayers measured had interface charges in the range $\sigma = (7-9) \times 10^{11}$ cm^{-2}. The germanium samples, on the other hand, had no detectable built-in fields. These samples were somewhat harder to measure due to the lack of insulating layers, leading to much lower breakdown fields. However, experiments done at $T = 20$ K showed that $|\phi_s| < 5$ meV, or $|\phi| < 2 \times 10^{11}$ cm^{-2}.

This rough comparison is consistent with the defect densities measured by other techniques. It is also in line with the degree of structural mismatch at the interface and the ability of the lattice to accommodate such mismatch. The silicon-germanium multilayers have been shown to have relatively defect-free interfaces by luminescence[35] and transport[36] measurements. Relatively speaking, silicon and germanium bulk lattices are very well matched both in terms of lattice constant and structure. The lattice constant is less well matched for the silicon carbide, and severly mismatched for silicon nitride. (The oxides will be treated separately below.) In fact, the silicon and silicon nitride lattices are so different both in structural type and interatomic spacing that it is difficult to imagine a well-constructed interface between the two of them. This is consistent with observations on the multilayer systems. Raman measurements[37,38] show a high level of interfacial disorder. Defects at the interfaces are passivated by 10^{15} cm^{-2} hydrogen atoms at the interface.[9] This hydrogen distribution peaks in the first monolayer and extends 19 Å into the a-Si:H layer. The silicon—silicon nitride superlattices are also transfer doped,[5] indicating that many of these defects are charged. In fact, the charged defect density we observed in electroabsorption of 6×10^{12} cm^{-2} (assuming all charges are at one interface) is still less than 1% of the excess hydrogen at that interface. Thus, almost all of the interface defects are passivated by hydrogen, as is true for bulk "dangling bond" defects in a-Si:H. Interface defects caused by lattice mismatch would be expected to depend strongly on the order of deposition,[10] as is observed in the electroabsorption experiments.

The sign of the built-in fields, in combination with the sign of the charges as measured in transfer doping, indicates that the charges are concentrated at the interface where silicon is deposited onto silicon nitride. This interface has also been shown to have a greater hydrogen interfacial concentration by photoemission.[39] This determination of greater defect density at the silicon-on-nitride interface in the multilayer system is opposite to measurements on single interfaces,[40] pointing out the importance of deposition conditions on interfacial properties.

Although the silicon—silicon oxide interface also has a large degree of lattice mismatch, the oxide is more able to

accommodate strain by bond-angle fluctuations than ni- trides. This is evidenced by the very high electronic quali- ty interfaces produced by thermal oxidation of crystalline silicon. The oxides also differ from the nitride system in that the oxide plasma can oxidize a silicon layer; this pro- cess is much slower for the nitrides. This introduces an interface asymmetry which is not present in the Si/SiN_x multilayers: one interface is a deposited one (silicon on oxide) while the other is an oxidized one (oxide on silicon). The fact that the interface properties observed depend very strongly on deposition parameters show that this asymmetry is responsible for a large part of the built-in potentials observed. The deposited interface probably differs from the oxidized one in several respects, such as stoichiometry and abruptness. Our results show that they also substantially differ in the conduction band mismatch. This asymmetry dominates any simple interface charges in the electroabsorption measurement.

In situ reflectivity measurements[34] have shown that these interfaces are rough, with ~ 10 Å roughness on a transverse scale length of ~ 100 Å. Note that this devia- tion from flatness does not preclude the interface being abrupt. The connection between this roughness and the interface charges described in this paper is uncertain at present. In any case, the roughness is too small to have a large effect on the built-in fields or our measurements of the interface defects.

VII. CONCLUSIONS

We have used electroabsorption spectroscopy to mea- sure built-in electric fields in amorphous multilayer sys- tems. In the silicon—silicon oxide system these fields can be accurately modeled by an asymmetric conduction band offset. The conduction band discontinuity is 170 meV greater when oxide is deposited onto silicon than in silicon-on-oxide interfaces. The silicon—silicon nitride system has large fields caused by charged interface de- fects. These charges are associated with the transfer- doping process and are asymmetric due to the presence of substantial lattice mismatch.

Electroabsorption complements other spectroscopic techniques in that it measures charged defects which are asymmetrically positioned. In superlattice systems the electroabsorption technique is very sensitive due to the large number of interfaces. These materials provide a convenient means for studying interfaces between a large number of semiconductors and insulators.

[1]M. J. Powell, Appl. Phys. Lett. 43, 597 (1983).

[2]J. Mort, F. Jansen, S. Grammatica, M. Morgan, and I. Chen, J. Appl. Phys. 55, 3197 (1984).

[3]B. Abeles and T. Tiedje, Phys. Rev. Lett. 51, 2003 (1983).

[4]N. Ibaraka and H. Fritzsche, Phys. Rev. B 30, 5791 (1984).

[5]T. Tiedje and B. Abeles, Appl. Phys. Lett. 45, 179 (1984).

[6]T. Tiedje, B. Abeles, and B. Brooks, Optical Effects in Amor- phous Semiconductors, Proceedings of the Conference on Op- tical Effects in Amorphous Semiconductors, Snowbird, 1984, AIP Conf. Proc. No. 120, edited by P. C. Taylor and S. G. Bishop (AIP, New York, 1984), p. 417.

[7]B. A. Wilson, Z E. Smith, C. M. Taylor, and J. P. Harbison, Solid State Commun. 55, 105 (1985).

[8]T. Tiedje, C. B. Roxlo, B. Abeles, and C. R. Wronski, Proceed- ings of the 16th International Conference on Solid State De- vices and Materials, Kobe, Japan, 1984, (unpublished), p. 531.

[9]B. Abeles, L. Yang, P. D. Persans, and H. C. Stasiewski, Appl. Phys. Lett. 48, 168 (1986).

[10]C. B. Roxlo, B. Abeles, and T. Tiedje, Phys. Rev. Lett. 52, 1994 (1984).

[11]C. B. Roxlo, T. Tiedje, and B. Abeles, in Optical Effects in Amorphous Semiconductors, Ref. 6, p. 433

[12]B. Abeles and T. Tiedje, Semiconductors and Semimetals, Vol. 21 (Academic, London, 1984), part c, p. 407.

[13]B. Abeles, T. Tiedje, K. S. Liang, H. W. Deckman, H. C. Stasiewski, J. C. Scanlon, and P. M. Eisenberger, J. Non- Cryst. Solids 66, 351 (1984).

[14]B. Abeles, P. D. Persans, and H. Stasiewski, Bull. Am. Phys. Soc. 30, 628 (1985).

[15]M. Cardona, Modulation Spectroscopy (Academic, New York, 1969).

[16]W. Franz, Z. Naturforsch. 13A, 484 (1958); L. V. Keldysh, Zh. Eksp. Teor. Fiz., 34, 962 (1958) [Sov. Phys.—JETP 34, 788 (1958)].

[17]B. Esser, Phys. Stat. Solidi (B) 51, 735 (1972).

[18]J. D. Dow and D. Redfield, Phys. Rev. B 5, 594 (1972).

[19]R. A. Street, T. M. Searle, I. G. Austin, and R. S. Sussmann, J. Phys. C 7, 1582 (1974).

[20]R. S. Sussmann, I. G. Austin, and T. M. Searle, J. Phys. C 8, L182 (1975).

[21]T. Noguchi, S. Usui, A. Sawada, Y. Kanoh, and M, Kikuchi, Jpn. J. Appl. Phys. 21, L485 (1982).

[22]S. A. Jalali and G. Weiser, J. Non-Cryst. Solids 41, 1 (1980).

[23]U. Mescheder and G. Weiser, Optical Effects in Amorphous Semiconductors, Ref. 6, p. 356.

[24]S. Nonomura, H. Okamoto, and Y. Hamakawa, Jpn. J. Appl. Phys. 21, L464 (1982).

[25]Y. Hamakawa, in Semiconductors and Semimetals, Vol. 21, Part B, edited by J. Pankove (Academic, London, 1984), p.141.

[26]I. Chen, Phys. Rev. B 32, 885 (1985).

[27]T. Tiedje, C. R. Wronski, B. Abeles, and J. M. Cebulka, Sol. Cells 2, 301 (1980).

[28]S. M. Sze, Physics of Semiconductor Devices (Wiley, New York, 1983).

[29]C. B. Roxlo, B. Abeles, and P. D. Persans, Appl. Phys. Lett. 45, 1132 (1984).

[30]P. D. Persans, A. F. Ruppert, B. Abeles, T. Tiedje, and H. Stasiewski, Phys. Rev. B 32, 5558 (1985).

[31]H. W. Deckman, J. Dunsmuir, and B. Abeles, Appl. Phys. Lett. 46, 171 (1984).

[32]R. Cheng, S. Wen, J. Feng, and H. Fritzsche, Appl. Phys.

Lett. **46**, 592 (1985).

[33]P. D. Persans, B. Abeles, H. Stasiewski, and J. Scanlon, *Proceedings of the 17th International Conference on the Physics of Semiconductors* (Springer-Verlag, New York, 1985), p. 499.

[34]L. Yang, B. Abeles, and P. D. Persans, Appl. Phys. Lett. (in press).

[35]T. Tiedje, B. Abeles, and B. G. Brooks, Phys. Rev. Lett. **54**, 2545 (1985).

[36]C. R. Wronski, P. D. Persans, and B. Abeles, Appl. Phys. Lett. (in press).

[37]N. Maley and J. S. Lannin, Phys. Rev. B **31**, 5577 (1985); Proceedings of the International Conference on Theory of Structure of Non-Cryst. Solids, Bloomfield Hills, 1985 (unpublished).

[38]B. Abeles, P. D. Persans, H. C. Stasiewski, L. Yang, and W. Lanford, J. Non-Cryst. Solids **77&78**, 1065 (1985).

[39]B. Abeles, I. Wagner, W. Eberhardt, J. Stohr, H. Stasiewski, and F. Sette, AIP Conf. Proc. **120**, 394 (1984).

[40]R. A. Street and M. J. Thompson, Appl. Phys. Lett. **45**, 769 (1984).